Structure of Human Parathyroid Hormone(1–34) in the Presence of Solvents and Micelles†

Lou Anne Strickland, Richard P. Bozzato, and K. Anne Kronis*

Allelix Biopharmaceuticals Inc., 6850 Goreway Drive, Mississauga, Ontario, Canada L4V 1P1

Received January 12, 1993; Revised Manuscript Received March 23, 1993

ABSTRACT: The structure of the N-terminal 34-residue fragment of human parathyroid hormone was determined in 40% trifluoroethanol employing two-dimensional ^{1}H nuclear magnetic resonance spectroscopy. The proton chemical shifts were assigned from magnitude and phase-sensitive COSY, relayed COSY, and NOESY spectra. Distance constraints, estimated from NOESY spectra, were used to create a set of structures by distance geometry (DGEOM) which were subsequently refined by restrained energy minimization and restrained molecular dynamics (CHARMm). The resulting structures contained two helices spanning residues 3–12 and residues 17–26. The NOE constraints for residues 13–16 did not provide a single structural solution; however, their conformations were not disordered. The structures prepared by DGEOM and refined with CHARMm contained either an irregular turn or a helical structure at residues 13–16. The secondary structure of human parathyroid hormone(1–34) was also assessed by circular dichroism in the presence of methanol, trifluoroethanol, and dodecylphosphocholine micelles. Under all three conditions, the peptide formed structures containing various amounts of helical content. The formation of helical secondary structure in the presence of micelles supports the proposal that the trifluoroethanol-induced structure of human parathyroid(1–34) was not an artifact of its environment but perhaps was an indication of the conformation that the molecule adopts when in close proximity to a membrane surface and possibly when bound to the parathyroid receptor.

Parathyroid hormone (PTH)[1] is the major regulator of extracellular calcium homeostasis (Potts *et al.*, 1982). Binding of the hormone to receptors on bone and kidney cells results in an increase in calcium blood levels. The major bioactive and circulating form of the hormone is the 84 amino acid peptide. The N-terminal 34 residues are sufficient for receptor binding and carry out most of the biological functions of the full-length molecule which include, at the cellular level, activation of adenylate cyclase. Sequence–activity studies using analogues and fragments have focused on identifying the regions important for activity and receptor binding in the first 34 residues (Caulfield & Rosenblatt, 1990). The N-terminus has been shown to be important for activation; fragments lacking the first two residues retain receptor binding ability but do not stimulate adenylate cyclase activity. In addition, specific binding sites have been identified for the midregion and C-terminus of the 84-residue hormone (McKee & Murray, 1985; Demay *et al.*, 1985). Elucidation of the three-dimensional, solution structure of the N-terminal, adenylate cyclase-active fragment of PTH provides a valuable tool for obtaining a better understanding of the structure–activity relationship between these domains.

Structural studies on PTH have employed dark-field electron microscopy, CD, fluorescence, and NMR. The microscopy studies indicated that the full-length hormone possessed two structural domains of different sizes connected by an extended linker (Fisken *et al.*, 1977). This is similar to the models which were prepared employing structure prediction methods (Zull & Naomi, 1980; K. A. Kronis, unpublished observation). In general, CD studies indicated that the hormone, in aqueous solution, was extended and mostly disordered. The spectra of both the full-length and the N-terminal 34-residue fragment have been reported to show some pH dependence (Salvatore & Edelhoch, 1972; Epand *et al.*, 1985b; Willis & Szabo, 1992). A similar trend was observed from fluorescence studies on hPTH(1–34) (Brewer *et al.*, 1974). Nonpolar solvents such as hexafluoro-2-propanol and TFE have been reported to induce helix formation (Nussbaum *et al.*, 1985; Cohen *et al.*, 1991). For both bPTH(1–34) and the C-terminal amide derivative of hPTHrP(1–34), a maximal helical content of approximately 25 residues was reportedly reached between 35 and 40% TFE.

Phospholipid vesicles have also been employed to induce secondary structure. The binding of hPTH(1–34) to DMPC and DMPG vesicles resulted in only small changes in the CD spectra, with DMPG causing the larger effect (Epand *et al.*, 1985a,b). More recently, the association of hPTH(1–34) with POPS vesicles was reported to induce a significant amount of α-helical content (Neugebauer *et al.*, 1992). The lack of ordered structure in aqueous solution and the induction of secondary structure by nonpolar solvents and phospholipids are characteristic features common to several peptide hormones which, like PTH, lack disulfide bonds. This is particularly true for those peptides capable of forming amphipathic helices (Segrest *et al.*, 1990).

The findings of the previously published NMR studies complement those of CD and fluorescence spectroscopies. The first one-dimensional ^{1}H NMR studies of hPTH(1–34) in

† This work was supported by Glaxo Canada Inc. L.A.S. was a recipient of a National Sciences and Engineering Research Council of Canada Industrial Research Fellowship.

* To whom correspondence should be addressed.

[1] Abbreviations: bPTH, bovine parathyroid hormone; CD, circular dichroism; CMC, critical micelle concentration; COSY, correlated spectroscopy; DMPC, dimyristoylphosphatidylcholine; DMPG, dimyristoylphosphatidylglycerol; DPC, dodecylphosphocholine; hPTH, human parathyroid hormone; hPTHrP, human parathyroid hormone related protein; MRE, mean residue ellipticity; NMR, nuclear magnetic resonance; NOE, nuclear Overhauser enhancement; NOESY, nuclear Overhauser and exchange spectroscopy; POPS, 1-palmitoyl-2-oleoylphosphatidylserine; RMS, root mean square; TFE, trifluoroethanol; TSP, 3-(trimethylsilyl)propionic acid.

0006-2960/93/0432-6050$04.00/0

aqueous solution revealed a predominantly extended and flexible structure with the only ordered region encompassing residues 20–24 (Bundi *et al.*, 1976, 1978). In a subsequent NMR study on bPTH(1–34), a small amount of secondary structure was postulated by observed spectral changes as a function of pH (Smith *et al.*, 1987). The first two-dimensional ^{1}H NMR study showed that in aqueous solution hPTH(1–34) had no detectable secondary structural elements (Lee & Russell, 1989), although some evidence for a nonlinear segment between residues 20 and 24 was presented. The structure of hPTHrP(1–34) was determined by NMR in an aqueous solution and reported to be surprisingly compact with an α-helix and two β-turns (Barden & Kemp, 1989). Eight of the first 13 residues of this peptide are identical to hPTH, and several biological activities are common to both peptides. hPTHrP binds to the same receptors as hPTH(1–34) and stimulates adenylate cyclase activity *in vitro* (Rabbani *et al.*, 1988).

Since the initiation of our studies, the three-dimensional structure of hPTH(1–34) in 10.7% TFE has been solved by NMR and reported independently (Klaus *et al.*, 1991). Under these conditions, the secondary structure was reported to consist of two α-helices extending from residues 3 to 9 and from residues 17 to 28. The two helices were joined by a disordered seven-residue linker. Due to the absence of NOEs between the two helices, their relative orientation was not determined. The authors reported that the amount of secondary structure induced by TFE, as measured by changes in α-proton and methyl proton chemical shifts, reached a maximum at a concentration of approximately 10–15% TFE.

Reported here are studies which demonstrate that hPTH(1–34) is capable of exhibiting more secondary and tertiary structure than previously described by Klaus *et al.* (1991). CD studies which show helical content in hPTH(1–34) increasing as a function of solvent concentration to 35–40% TFE or 100% MeOH are presented. Also described are NMR studies on hPTH(1–34) in 40% TFE which include analysis of the resulting structures. These structures were found to be highly helical with their global conformations falling into one of two families. As well, CD studies are described that demonstrate helix stabilization in hPTH(1–34) by DPC micelles.

MATERIALS AND METHODS

Chemicals. hPTH(1–34) was purchased from Bachem Inc. (Torrance, CA) and used without further purification. The peptide purity was greater than 99% by HPLC analysis. Spectral-grade trifluoroethanol and methanol were used in the CD studies without further purification. Dodecylphosphocholine-d_{38} was purchased from MSD Isotopes (Pointe Claire-Dorval, Quebec, Canada). TFE-d_3 (99%) and D_2O (99.96%) were purchased from Cambridge Isotopes Ltd. (Woburn, MA).

CD Spectroscopy. Far-UV CD spectra of approximately 0.1 mg/mL solutions of hPTH(1–34) were measured using a 0.1-cm path-length cell in a Jasco J-720 spectropolarimeter. The data were collected and processed on a personal computer using the Jasco 700 software. The peptide was initially solubilized in 10 mM acetic acid and then diluted with water, TFE, MeOH, or, for the DPC studies, 40 mM phosphate buffer (pH 7.0). The final phosphate buffer concentration was 10.3 mM. The solvent concentrations were reported as percent volume. The peptide concentrations of the solutions analyzed were determined from the UV absorbance at 280 nm using a molar extinction coefficient of 5690 M^{-1} cm^{-1}. This assumes that tryptophan-23 is the only factor contributing to the UV absorbance at this wavelength. The mean residue ellipticity was calculated using the mean residue molecular mass of hPTH(1–34), namely, 121 daltons.

NMR Spectroscopy. All two-dimensional NMR spectra were collected using samples containing approximately 10 mM hPTH(1–34) in either solution A (40% TFE-d_3 and 60% D_2O) or solution B (40% TFE-d_3, 6% D_2O, and 54% H_2O). Typically, three or four two-dimensional NMR spectra were accumulated on a given sample in solution A or B during a 60-h period. The samples were prepared within a few hours of the initiation of data collection and were lyophilized at the end of the block of time. The dry peptide was stored at −20 °C between NMR experiments. All spectra were recorded on a Bruker AM 500 spectrometer at 300 K. Resonance assignments were made from a magnitude COSY (Aur *et al.*, 1976) spectrum in solution A, a phase-sensitive COSY (Marion & Wuthrich, 1983) spectrum in solution B, and MLEV-17 (Bax & Davis, 1985) spectra in solution B with mixing times of 50, 75, and 100 ms. Phase-sensitive NOESY (Bodenhausen *et al.*, 1984) spectra were collected in solution B with mixing times of 100 and 200 ms and in solution A with a mixing time of 200 ms. Spectra collected in solution B were presaturated using the Bruker Presat program at the appropriate power level. All proton chemical shifts were referenced relative to TSP-d_4. Application of window functions, phasing, transformation, and analysis were done using the FELIX software package (Hare Research Inc., Woodinville, WA).

Structure Determination. Analysis of the NOESY spectra resulted in 145 interresidue distance constraints which were classified into 3 categories, namely, strong ($\leq$ 3.0 Å), medium ($\leq$4.0 Å), and weak ($\leq$5.0 Å). The peak volumes were calibrated against peaks resulting from known interproton distances. The lower limit of the range used for the distance constraints was 1.2 Å for distance geometry calculations and 1.5 Å for restrained energy minimization and restrained molecular dynamics calculations. When these constraints were employed, 150 structures were prepared by distance geometry using DGEOM (Blaney *et al.*, 1990). The 10 structures with the smallest total RMS difference between the NOE distance constraints and the actual distances in the structure were selected for further analysis. These structures were refined with 100 steps of restrained energy minimization using a steepest descent gradient, updating the nonbonded contacts every 20 steps. A distance limit of 15 Å was used for the van der Waals and electrostatic interactions by employing a switching algorithm. The dielectric constant was maintained at a value of 1. The minimized structures were further refined by restrained molecular dynamics. This involved 3 ps of heating to 300 K followed by 5 ps of equilibration and 15 ps of dynamics simulation at this temperature. Coordinate sets and energy terms were saved every 0.1 ps during the simulation. Bond lengths involving hydrogen atoms were maintained with the SHAKE algorithm (van Gunsteren & Berendsen, 1977). Both restrained energy minimization and restrained molecular dynamics calculations were done using CHARMm 21.3 (Brooks *et al.*, 1983) and the results displayed and analyzed using the QUANTA 3.2.1 software package (Molecular Simulations, Sunnyvale, CA).

RESULTS

CD Spectroscopy. The CD spectrum of hPTH(1–34) was measured in various concentrations of TFE and MeOH. The MRE at 208 and 222 nm for hPTH(1–34) increased negatively as a function of solvent concentration. The MRE minimum

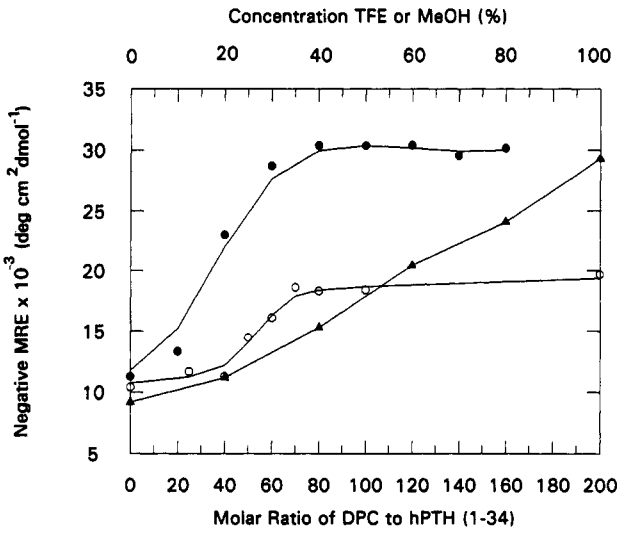

FIGURE 1: Negative mean residue ellipticity (MRE) of hPTH(1–34) at 208 nm in various concentrations of MeOH (▲), TFE (●), and DPC (○). The data points were taken from representative scans collected at room temperature.

at 203 nm shifted to 208 nm as the concentration of solvent increased.

The negative MRE at 208 nm was plotted as a function of TFE or MeOH concentration (Figure 1). This value is taken to be representative of the helical content in peptides and proteins (Adler *et al.*, 1973). Other secondary structural elements, however, do contribute to the ellipticity at this wavelength. Therefore, the data in Figure 1 have been interpreted as an indication of the relative change in the helical content and will be discussed without assigning the percentage of residues in a helical conformation. The negative MRE at 208 nm for hPTH(1–34) in TFE increased until the solvent concentration reached between 30% and 40%, at which point it became constant. This indicated a transition from a set of disordered structures, at 0% TFE, to a set of structures with a significant amount of helical content at or above 40% TFE. The negative MRE at 208 nm from the MeOH titration gradually increased as the MeOH concentration was varied from 0% to 100% (see Figure 1). The transition from disordered structures to ordered, helical structures in the presence of increasing amounts of MeOH was less dramatic than was observed with TFE.

The CD spectra of hPTH(1–34) were also measured in the presence of DPC at concentrations spanning its CMC. The DPC micelle environment mimics that of a lipid membrane more closely than do solvents. The MRE at 208 nm was plotted as a function of the molar ratio of DPC to hPTH(1–34) in Figure 1. At DPC concentrations below the critical micelle concentration [CMC = 1.0 mM or, under these conditions, at a ratio of 44 DPC molecules to 1 hPTH(1–34) molecule], small changes in the CD spectra were observed as the DPC concentration increased. Above the CMC, the MRE increased negatively, forming minima at 208 and 222 nm, which indicated an increase in helical structure. This trend continued until the DPC concentration reached a molar ratio of 70 DPC to 1 hPTH(1–34). The MRE at 208 nm remained constant from a molar ratio of 70 DPC to 1 hPTH(1–34) to the highest molar ratio tested [500 DPC to 1 hPTH(1–34); data not shown]. The interaction between the peptide and the micelles was found to be stable for at least 4 h and was independent of pH in the range of 5–9 (data not shown).

2-D NMR Spectroscopy. The chemical shifts were assigned by using two-dimensional COSY, relayed COSY, and NOESY spectra and by following established procedures. All of the protons of hPTH(1–34) were assigned uniquely with the exception of a few belonging to residues 7 and 29. The chemical shifts for the assigned protons are listed in Table I. Thirty-two peaks representing coupling between the amide and α-protons were present in the phase-sensitive COSY (Figure 2). Peaks for residues 1 and 29 were not observed in this region of the spectrum. A NOESY spectrum acquired under identical conditions showed the same 32 peaks as well as several peaks due to interresidue NOEs.

The α-proton of S1 was assigned from its NOE to the amide proton of V2. The α-proton of E29 could not be assigned. However, the amide proton of E29 was assigned from its NOE to the amide proton of L28. The β-protons of E29 were assigned from NOEs to their own amide proton and to the amide proton of N30. Several NOEs were observed between α- and β-protons and between α-protons and amide protons of adjacent residues. In addition, there were 28 NOEs which resulted from the interaction of amide protons with amide protons of the adjacent residues. These peaks assisted in the sequential assignment of most residues (see Table I).

Aromatic residues, H9, H14, and W23, were readily assigned by NOE peaks between backbone and ring protons. The assignment of H32 and F34 was more difficult due to the lack of NOEs between backbone and side chain protons. The indole ring protons of W23 exhibited several easily identifiable NOEs to L24 side chain protons, and, therefore, W23 was used as a starting point for sequential assignments.

The observed interresidue NOEs, which characterize secondary structural elements, have been summarized in Figure 3. The large numbers of NOEs observed between the α-protons of residue i and either the β-protons or amide protons of residue $i+3$ are indicative of α-helical secondary structure (Wuthrich, 1986). An N-terminal region spanning residues 3–12 exhibited most of the predicted NOEs for an α-helix. The beginning of a second helix was identified by an NOE between the α-proton of residue 17 and the amide proton of residue 20. The NOEs characteristic of α-helices extended for approximately 10 residues C-terminal to residue 17 (see Figure 3).

Structure Preparation. A total of 145 interresidue NOEs (see for example Figure 3) were used to calculate 150 structures by distance geometry. The RMS difference between the NOE constraints and the actual interproton distances for each structure was calculated and used as a measure of the agreement between the structures and the NMR data. The 10 structures with the smallest RMS difference (<0.91 Å) were identified. Their CHARMm energies (Momany & Rone, 1992) were calculated and found to be positive. Refinement with restrained energy minimization, employing the 145 NOEs as distance constraints, lowered the CHARMm energies to negative values. This step removed virtually all close, nonbonded contacts between side chain atoms. Restrained molecular dynamics simulations were performed subsequently on each structure using the same set of 145 distance constraints. This step further lowered the CHARMm energy of each structure.

Average structures were prepared from the final 5 ps of each dynamics run using QUANTA. These were minimized without constraints for 100 cycles with a steepest descent gradient to correct the artifacts, such as distorted bond lengths and angles, which resulted from averaging coordinates. These average structures were used as reference points for assessing the flexibility and conformational space experienced by the molecule during restrained molecular dynamics. This analysis

Table I: Proton Shifts (ppm) for hPTH(1–34) in 40% TFE Referenced to TSP

residue		HN	αH	βH	γH	δH	other
Ser	1		4.14	4.02, 3.97			
Val	2	8.54	4.03	1.99	0.91, 0.87		
Ser	3	8.15	4.38	3.93, 3.82			
Glu	4	8.27	3.96	2.07, 2.01	2.36, 2.26		
Ile	5	7.56	3.71	1.79	1.13, 1.52	0.78, 0.77	
Gln	6	7.75	3.92	2.28, 2.06	2.51, 2.65		
Leu	7	7.99	4.04	1.70, 1.57		0.82, 0.79	
Met	8	8.36	4.15	2.15, 1.99	2.52, 2.65		
His	9	8.33	4.32	3.27, 3.34			2H 8.44, 4H 7.25
Asn	10	8.28	4.45	2.93, 2.78			γNH_2 6.85, 7.17
Leu	11	8.72	4.09	1.70, 1.63	1.57	0.80, 0.74	
Gly	12	8.40	3.81				
			3.69				
Lys	13	7.91	4.02	1.80, 2.08	1.31, 1.43	1.57, 1.76	ϵH 3.06, 2.84; ϵNH_3 6.97
His	14	8.02	4.31	3.34, 3.31			2H 8.54, 4H 7.16
Leu	15	8.60	4.07	1.73, 1.67	1.53	0.81, 0.78	
Asn	16	8.25	4.36	2.83, 2.64			
Ser	17	7.89	4.14	3.85, 3.99			
Met	18	7.96	4.10	2.16, 2.07	2.35, 2.47		
Glu	19	8.22	3.92	2.14, 2.02	2.52, 2.33		
Arg	20	7.73	4.01	1.80, 1.92	2.02, 1.58	2.84, 3.06	HN 6.98
Val	21	7.80	3.67	2.16	1.01, 0.87		
Glu	22	8.10	3.95	2.08, 2.16	2.38, 2.47		
Trp	23	8.23	4.14	3.47, 3.30			2H 7.11, 4H 7.50, 5H 6.96, 6H 7.01, 7H 7.33
Leu	24	8.27	3.79	1.76, 1.71	1.69	0.86, 0.73	
Arg	25	8.44	3.77	1.82, 1.71	1.79, 1.48	3.02, 3.13	
Lys	26	7.76	3.88	1.77, 1.97	1.52, 1.44	1.57, 1.30	ϵH 2.85
Lys	27	7.88	3.82	1.58, 1.46	1.30, 1.55	1.79	ϵH 3.05; ϵNH_3 6.96, 6.52
Leu	28	8.24	4.00	1.37, 1.30	1.73	0.83, 0.71	
Gln	29	7.75		2.07, 2.27	2.39		γNH_2 7.20, 6.54
Asp	30	7.91	4.55	2.82, 3.01			
Val	31	7.69	3.86	2.02	0.83, 0.75		
His	32	7.99	4.49	3.13, 2.97			2H 8.40, 4H 7.14
Asn	33	7.98	4.59	2.59, 2.65			γNH_2 7.34, 6.60
Phe	34	7.69	4.48	3.08, 2.95			3H,5 7.20; 4H 7.14; 2H,6 7.15, 7.11

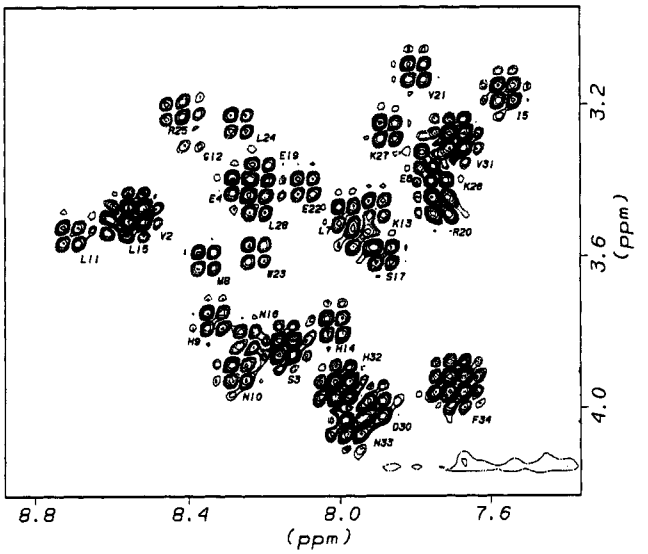

FIGURE 2: Backbone proton region of the phase-sensitive COSY spectrum collected on hPTH(1–34) in 40% TFE-d_3, 6% D_2O, and 54% H_2O at 300 K.

was carried out on 5 coordinate sets chosen at random from the last 5 ps of each of the 10 dynamics simulations. These structures were fit to their average structure by a least-squares minimization procedure covering the region from residues 5 to 26. The RMS difference per residue, between each of the five coordinate sets and its average minimized structure, was calculated. An example of this type of analysis is given in Figure 4 where the RMS difference was plotted as a function of the residue number for five coordinate sets from one dynamics run. Analyses of all 10 dynamics runs using this method showed that the RMS differences remained below 1.0 Å between residues 4 and 26. Thus, this region exhibited little flexibility. Higher RMS differences were calculated for residues at both the N- and C-termini. This arises from a lack of interresidue NOEs in these regions. An absence of NOEs is in turn characteristic of a highly flexible or disordered region.

A comparison of the backbone conformations of the structures resulting from each of the 10 dynamics runs was performed. The backbone atoms of various regions in the 10 different structures were fit to each other using least-squares minimization of the RMS difference. The RMS difference for that region was used as a measure of the similarity in conformations between the 10 structures in different regions. Regions with similar conformations in all 10 structures gave lower RMS values than regions which included residues with different conformations. From this analysis, it was apparent that there were 2 conserved domains in all 10 structures. These corresponded to two α-helices spanning residues 3 through 12 and residues 17 through 26. The region between residues 13 and 16 had different conformations in each structure as indicated by higher RMS differences. The secondary structure of this region is described in more detail below. The N- and C-termini also had regions which differed in conformation between the 10 structures.

Figure 5 shows an example of the analysis described above in which the N-terminal helix-spanning residues 3 through 12 from the 10 restrained dynamics structures were fit to each other. Least-squares fitting of the second helix (residues 17–26; Figure 6) did not result in as low an RMS difference as

FIGURE 3: NOEs between residues of hPTH(1–34). The NOEs were measured from peak volumes of phase-sensitive NOESY spectra collected in 40% TFE-d_3, 6% D_2O, and 54% H_2O or in 40% TFE-d_3 (99%) and 60% D_2O (99.96%) at 300 K, both with mixing times of 200 ms. The NOEs are classified as strong (≤3.0 Å) (thick black boxes), medium (≤4.0 Å) (thin black boxes), and weak (≤5.0 Å) (—).

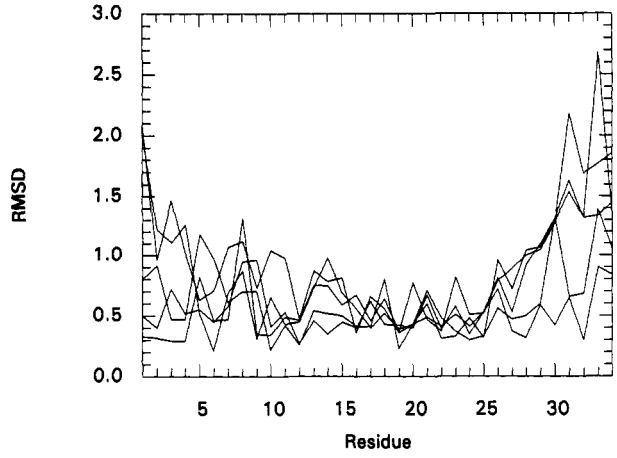

FIGURE 4: RMS difference (RMSD) per residue of hPTH(1–34) between five sets of coordinates from the last 5 ps of a restrained molecular dynamics run and the average structure prepared from all coordinate sets in the last 5 ps of the same dynamics run.

was obtained for the first helix. This indicated that small differences existed between structures in the region of residues 17–26. The ϕ and ψ angles for this region, however, were mostly in the helical range with a few anomalies. These included carbonyls which were oriented in the direction opposite to that expected for an α-helix. The C-terminal helix did not terminate at the same residue in each of the 10 structures. In 6 of the 10 structures, there were kinks in the helix at residue 26. The residues C-terminal to the kinks were disordered. In the other four structures, the α-helix ended at either residue 24 or residue 28.

In 40% TFE, no NOEs were detected between the two helical domains. This prohibited uniquely defining the relative orientation of the two helices. Their relative position, therefore, was dependent upon the conformation of residues 13–16. NOEs between the α-protons of residue i and the β-protons of residue i+3, which are indicative of helical conformations, existed throughout the region joining the helices (see Figure 3). However, NOEs between α-protons of residue i and the amide protons of residue i+3, which are also present in α-helices, were not observed. This is consistent with the different conformations observed for residues 13 through 16 in the structures from the 10 dynamics runs. Of the 10 structures, 5 had irregular helical structures in the region of residues 13–16, resulting in a fairly linear tertiary structure (see Figures 5 and 6). The conformation of residues 13–16 in these five structures varied from a 3_{10}-helix to a kinked α-helix. The other five structures contained a bend or an irregular turn in this segment which resulted in structures which curved toward one face (see Figure 5).

DISCUSSION

The CD studies summarized in this work for hPTH(1–34) in the presence of both TFE and MeOH indicated an increase in helical content as the concentration of solvent increased and, therefore, as the dielectric constant decreased. This decrease in solvent polarity results in the amide protons adopting intramolecular hydrogen bonds as opposed to forming hydrogen bonds with the solvent (Nelson & Kallenbach, 1986). This was accomplished by helix formation.

The CD spectra of hPTH(1–34) in 10% and 40% TFE, shown in Figure 7, are similar in shape to the spectra of helical peptides such as poly(L-lysine) at pH 11 but exhibited different MRE values (Adler *et al.*, 1973). The spectrum of hPTH(1–34) in 40% TFE is shifted toward greater negative MRE values relative to the spectrum in 10% TFE. This corresponded to a higher percentage of the residues of hPTH(1–34) being helical in 40% TFE than in 10% TFE.

CD curves of hPTH(1–34) in the presence of DPC micelles also indicated the presence of helical secondary structure (see Figure 7). Spectra having the greatest negative MRE values in the far-UV [≥70 DPC:1 hPTH(1–34)] lie midway between the spectra collected in 10% TFE and 40% TFE (see Figure 7). This indicated that the helical content of hPTH(1–34) under these conditions was greater than that in 10% TFE and less than that in 40% TFE.

At and above a molar ratio of 70 DPC to 1 hPTH(1–34), the MRE values between 190 and 250 nm remained constant, indicating that the average of the helical content from all conformations present was constant. One interpretation could be that all peptide molecules were bound to the micelles. CD spectra collected at lower molar ratios of DPC to peptide could, therefore, represent averages of micelle-bound and -free conformations. The fact that little secondary structure was present at concentrations of DPC below its CMC implied that it was not the presence of DPC monomers but rather the DPC micelles which stabilized secondary structure in hPTH(1–34). Hormone secondary structure has been postulated to be stabilized during interaction with the cell membrane prior to specific receptor binding (Sargent & Schwyzer, 1986). Since

FIGURE 5: Stereo diagram depicting 10 structures of hPTH(1–34) overlayed by minimizing RMS differences between backbone atoms of residues 3–12. The structures were refined by restrained energy minimization and restrained molecular dynamics from the best 10 distance geometry calculations. The N-terminus is at the bottom in this view.

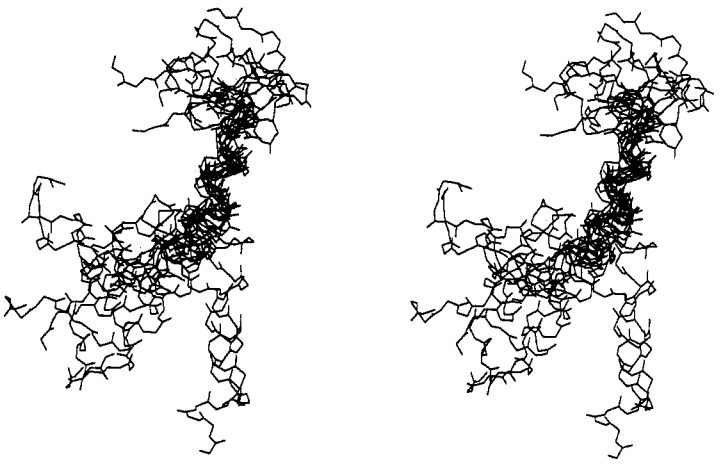

FIGURE 6: Stereo diagram depicting 10 structures of hPTH(1–34) overlayed by minimizing RMS differences between backbone atoms of residues 17–26. The structures were refined by restrained energy minimization and restrained molecular dynamics from the best 10 distance geometry calculations. The N-terminus is at the bottom in this view.

DPC micelles do to some extent mimic a cell membrane and both TFE and DPC micelles stabilize helix formation, one might therefore conclude that the receptor-bound conformation of hPTH(1–34) contains a significant amount of α-helical structure.

Stabilization of helical secondary structure by both TFE and DPC micelles is encouraging in light of concerns that TFE may induce α-helix formation in a nonselective fashion (Sönnichsen *et al.*, 1992). In our study, it appears that α-helical formation is a characteristic of hPTH(1–34) and not the environment used to induce ordered structure. In a recent study of actin peptides, it was shown that TFE stabilized α-helices only in regions with a propensity for α-helix formation (Sönnichsen *et al.*, 1992). TFE, in this study, was unable to induce α-helix in regions which were predicted to prefer nonhelical secondary structures.

The three-dimensional structure of hPTH(1–34) has now been determined by NMR methods in two different concentrations of TFE (this work; Klaus *et al.*, 1991). Although there are similarities between the resulting structures, the differences are significant. The structures prepared from NMR data collected in 40% TFE contained a higher degree of order than the structures prepared from 10.7% TFE. Both sets of structures contained two helical domains. In all of the structures prepared from 40% TFE, the N-terminal helix extended from residues 3 to 12. The length of this helix is consistent with the consensus structure obtained using eight secondary structure prediction algorithms (K. A. Kronis, unpublished observation). In the structures from 10.7% TFE, this helix was three residues shorter, extending only from residues 3 to 9 (Klaus *et al.*, 1991).

The C-terminal helix began at residue 17 in all structures prepared from both 40% TFE and 10.7% TFE. This helix terminated at residue 26 in the majority of the structures prepared from 40% TFE. In the other structures from this data set, the C-terminal helix ended either at residue 24 or at residue 28. In the structures prepared from 10.7% TFE, this helix ended at residue 28 (Klaus *et al.*, 1991). The residues at the N- and C-termini which were either before or after the helical domains were random in both of the structures prepared from 10.7% TFE and 40% TFE.

The conformation of the residues joining the two helical domains (residues 13 through 16) in the structures prepared from 40% TFE can be categorized into two families. In five of the structures, these residues formed an irregular turn or bend. In the remaining five structures, they took on some form of helical structure (i.e., 3_{10}- or α-helix). Examination of the backbone dihedral angles also indicated that there were

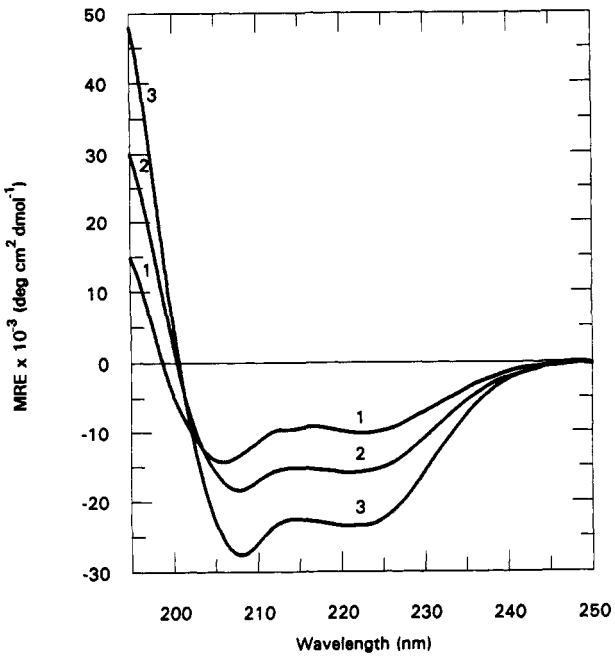

FIGURE 7: Molar ellipticity of hPTH(1–34) at room temperature in 10% TFE (1), 40% TFE (3), and at a molar ratio of 100 DPC to 1 hPTH(1–34) (2).

two conformational families for residues 13 through 16. For example, the ϕ angles for residue 16 in all of the bent structures were positive with a mean of 40° ± 40° while in the linear structures the ϕ angles were all negative with a mean of −50° ± 30° (data not shown). The conformation of residues 13 through 16 defined the relative orientation of the two helices and therefore the global conformation of the peptide (see Figure 5). Visual examination of these structures showed that there were two families of structures which resulted from the two families of conformations observed for residues 13 through 16. The structures with the bend or irregular turn in this region gave a family of structures that were all bent in one direction. The second family of structures were relatively linear with either a bulge or a kink in the region of residues 13 through 16.

The two helices in the structures prepared from 10.7% TFE were joined by a seven-residue disordered linker extending from residues 10 to 16 (Klaus *et al.*, 1991). The relative orientation of the two helices, therefore, was not defined under those conditions.

A comparison of the NOEs from spectra collected in 40% TFE and in 10.7% TFE revealed that there were additional NOEs, particularly those indicative of α-helices, in the data obtained at the higher TFE concentration (see Figure 3 for those obtained in 40% TFE). For example, there were eight NOEs between α-protons of residue i and β-protons of residue i+3 in the region of residues 4 through 17 which were not reported from the spectra collected in 10.7% TFE (Klaus *et al.*, 1991). These additional NOEs resulted in a more ordered secondary structure extending from residues 10 through 16 for the structures prepared from 40% TFE.

There were NOEs from the α-protons of residue i to the β-protons and amide protons of residue i+3 which were present in the data collected in 10.7% TFE yet were absent in the data collected in 40% TFE. These were almost entirely at the end of the second helix. For example, the NOEs between the α-protons on residues 24, 25, and 26 and the amide protons of residues 27, 28, and 29, respectively, were not observed in the data set in 40% TFE while they were in the data set from

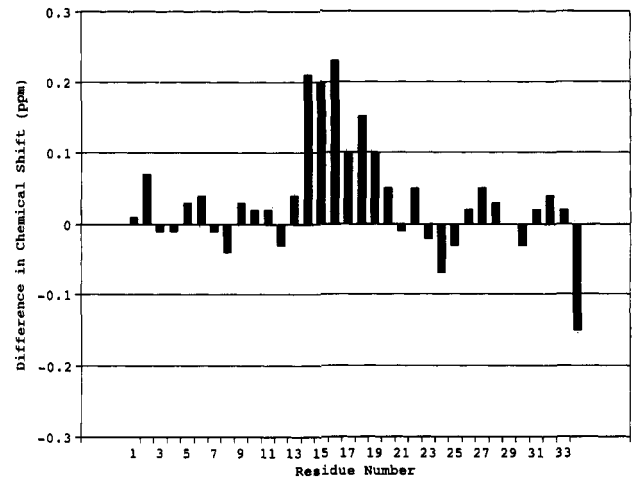

FIGURE 8: Difference in chemical shift (ppm) between the α-protons of hPTH(1–34) in 10.7% TFE (Klaus *et al.*, 1991) and in 40% TFE. The difference was calculated by subtracting the chemical shift in 40% TFE from the chemical shift in 10.7% TFE.

10.7% TFE (Klaus *et al.*, 1991). This resulted in the shorter C-terminal helix of a variable length in the structures prepared from 40% TFE.

α-Proton chemical shifts have been shown to be indicative of secondary structure (Wishart *et al.*, 1992). The difference in the α-proton chemical shifts between the spectra collected in 10.7% TFE (Klaus *et al.*, 1991) and the spectra obtained in 40% TFE (this study) is plotted in Figure 8 as a function of residue number. The difference in the chemical shift for most α-protons from residues 3 through 13 and residues 20 through 33 was very small (<0.05 ppm). Both sets of data resulted in structures which had similar secondary structural features in these regions with the exception of residues 10–13. The difference between the α-proton chemical shifts for residues 14, 15, and 16 was greater than 0.2 ppm and for residues 17, 18, and 19 was greater than 0.1 ppm, with the structure in 40% TFE having the higher field value in every case. The upfield shifts were toward values indicative of α-helical structure and away from those for random coils (Wishart *et al.*, 1992). This is consistent with the higher degree of order observed for this region in the structures prepared from 40% TFE compared with those from 10.7% TFE.

The only apparent discrepancy between the structural data presented in this study and previously published structures of PTH or its related molecule was with the structure of hPTHrP(1–34) determined by two-dimensional NMR in an aqueous solution (Barden & Kemp, 1989). This peptide, in which 8 of the first 13 residues are identical to hPTH(1–34), was reported to have a highly ordered, compact structure in water. The structure reported by Barden and Kemp (1989) is also inconsistent with structural information from CD studies of hPTHrP(1–34) in water and in 45% TFE (Cohen *et al.*, 1991). Since both hPTH(1–34) and hPTHrP(1–34) bind to the same receptor and have a similar bioactivity profile *in vitro*, a close structural similarity might be assumed. Therefore, it is difficult to reconcile the compact structure which was reported for hPTHrP(1–34) in water (Barden & Kemp, 1989) with the disordered conformation observed for hPTH(1–34) in water (Lee & Russel, 1989; this work). The degree of compactness and order reported for hPTHrP(1–34) was not observed with hPTH(1–34) even in the presence of 40% TFE. In light of the reported compact structure of hPTHrP(1–34), the spectra in this study were examined closely for NOEs which would represent close contacts between these regions,

but none were observed. The reasons for this discrepency remain unexplained.

In conclusion, TFE, MeOH, and DPC micelles are all capable of stabilizing helix formation in hPTH(1–34) as was determined by CD. Two helical domains were identified from residues 3 through 12 and from amino acid 17 through to residues 26, 27, or 28 in the structures of hPTH(1–34) in 40% TFE prepared from the NMR data. In these structures, the helices were joined by four residues whose conformations were not uniquely defined; however, they did demonstrate some order. The conformation of this region defines the relative orientation of the helices and therefore the tertiary structure of the peptide which corresponded to two families of conformers. Further refinement of the relative orientation of these helices may require structural studies in the presence of the PTH receptor. At present, this is a technically challenging task. Defining the structure of hPTH when bound to its receptor will enhance our understanding of the structure–activity relationships of the hormone. Although the tertiary structure has yet to be uniquely defined, the two families of structures presented here likely provide a clue as to the nature of the receptor-bound structure.

ACKNOWLEDGMENTS

We thank Drs. J. P. Carver and A. A. Grey, Department of Medical Genetics, University of Toronto, for the use of the 500-MHz NMR spectrometer and Dr. G.-Y. Xu for technical advice. In addition, we thank Dr. D. Isenman, Department of Biochemistry, University of Toronto, and Dr. C. Deber and Ms. M. Glibowicka, Department of Biochemistry, Hospital for Sick Children, for the use of the CD spectrometers and their technical assistance. As well, we extend our thanks to Dr. D. Rose, Department of Medical Biophysics, University of Toronto, for allowing us to use the Ontario Cancer Institute's computing facilities to perform the DGEOM calculations.

REFERENCES

Adler, A. J., Greenfield, N. J., & Fasman, G. D. (1973) *Methods Enzymol. 27*, 675.

Aur, W. P., Bartholdi, E., & Ernst, R. R. (1976) *J. Chem. Phys. 64*, 2229.

Barden, J. A., & Kemp, B. L. (1989) *Eur. J. Biochem. 184*, 379.

Bax, A., & Davis, D. G. (1985) *J. Magn. Reson. 65*, 355.

Blaney, J. M., Crippen, G. M., Dearing, A., & Dixon, J. S. (1990) QCPE Program No. 590.

Bodenhausen, G., Kogler, H., & Ernst, R. R. (1984) *J. Magn. Reson. 58*, 370.

Brewer, H. B., Fairwell, T., Werner, R., Littledike, T., & Arnaud, C. D. (1974) *Am. J. Med. 56*, 759.

Brooks, B. R., Bruccoleri, R. E., Olafson, B. D., States, D. J., Swaminathan, S., & Karplus, M. (1983) *J. Comput. Chem. 4*, 187.

Bundi, A., Andreatta, R., Rittel, W., & Wuthrich, K. (1976) *Fed. Eur. Biol. Sci. Lett. 64*, 126.

Bundi, A., Andreatta, R., & Wuthrich, K. (1978) *Eur. J. Biochem. 91*, 201.

Caulfield, M. P., & Rosenblatt, M. (1990) *Trends Endocrinol. Metab. 1*, 164.

Cohen, F. E., Strewler, G. J., Bradely, M. S., Carlquist, M., Nilsson, M., Ericsson, M., Ciardelli, T. L., & Nissenson, R. A. (1991) *J. Biol. Chem. 266*, 1997.

Demay, M., Mitchell, J., & Goltzman, D. (1985) *Am. J. Physiol. 249*, E437.

Epand, R. M., Epand, R. F., Hui, S. W., He, N. B., & Rosenblatt, M. (1985a) *Int. J. Pept. Protein Res. 25*, 594.

Epand, R. M., Epand, R. F., Orlowski, R. C., Flanigan, E., & Stahl, G. L. (1985b) *Biophys. Chem. 23*, 39.

Fiskin, A. M., Cohn, D. V., & Peterson, G. S. (1977) *J. Biol. Chem. 252*, 8261.

Klaus, W., Dieckmann, T., Wray, V., Schomberg, D., Wingender, E., & Mayer, H. (1991) *Biochemistry 30*, 6936.

Lee, S. C., & Russell, A. F. (1989) *Biopolymers 28*, 1115.

Marion, D., & Wuthrich, K. (1983) *Biochem. Biophys. Res. Commun. 113*, 967.

McKee, M. D., & Murray, T. M. (1985) *Endocrinology 117*, 1930.

Momamy, F. A., & Rone, R. (1992) *J. Comput. Chem. 13*, 888.

Nelson, J. W., & Kallenbach, N. R. (1986) *Proteins: Struct., Funct., Genet. 1*, 211.

Neugebauer, W., Surewicz, W. K., Gordon, H. L., Somorjai, R. L., Sung, W., & Willick, G. E. (1992) *Biochemistry 31*, 2056.

Nussbaum, S. R., Beaudette, N. V., Fasman, G. D., Potts, J. T., Jr., & Rosenblatt, M. (1985) *J. Protein Chem. 4*, 391.

Potts, J. T., Jr., Kronenberg, H. M., & Rosenblatt, M. (1982) *Adv. Protein Chem. 35*, 323.

Rabbani, S. A., Mitchell, J., Roy, D. R., Hendy, G. N., & Goltzman, D. (1988) *Endocrinology 123*, 2709.

Salvatore, A., & Edelhoch, H. (1972) *Arch. Biochem. Biophys. 150*, 782.

Sargent, D. F., & Schwyzer, R. (1986) *Proc. Natl. Acad. Sci. U.S.A. 83*, 5774.

Segrest, J. P., De Loof, H., Dohlman, J. G., Brouillette, C. G., & Anantharamaiah, G. M. (1990) *Protein: Struct., Funct., Genet. 8*, 103.

Smith, L. M., Jentoft, J., & Zull, J. E. (1987) *Arch. Biochem. Biophys. 253*, 81.

Sönnichsen, F. D., Van Eyk, J. E., Hodges, R. S., & Sykes, B. D. (1992) *Biochemistry 31*, 8790.

van Gunsteren, W. F., & Berendsen, H. J. C. (1977) *Mol. Phys. 34*, 1311.

Willis, K. J., & Szabo, A. G. (1992) *Biochemistry 31*, 8924.

Wishart, D. S., Sykes, B. D., & Richards, F. M. (1992) *J. Mol. Biol. 222*, 311.

Wuthrich, K. (1986) in *NMR of Proteins and Nucleic Acids*, pp 163–175, John Wiley & Sons, New York.

Zull, J. E., & Naomi, B. L. (1980) *Proc. Natl. Acad. Sci. U.S.A. 77*, 3791.